AGU ADVANCING EARTH AND SPACE SCIENCES

JGR Atmospheres

RESEARCH ARTICLE
10.1029/2025JD045745

Special Collection:
Extreme Hydrometeorological Events Under Climate Change: Past, Present, and Future

Key Points:

- Through data assimilation of $\delta^{18}O$ and precipitation, the hydroclimatic characteristics of the 4.2 ka event are reconstructed
- Mean shifts show drought in northern China and South Asia and wetness in southern China, remaining within the Holocene variability
- Drought and flood excursions are common across the Asian monsoon region, yet they generally fall below the threshold of extreme events

Supporting Information:

Supporting Information may be found in the online version of this article.

Correspondence to:

L. Ning,
ningliangnnu@njnu.edu.cn

Citation:

Xing, F., Ning, L., Liu, Z., Liu, J., Mann, M. E., Wu, F., et al. (2026). Precipitation reconstruction in the Asian monsoon region during the 4.2 ka event with paleoclimate data assimilation. *Journal of Geophysical Research: Atmospheres*, *131*, e2025JD045745. https://doi.org/10.1029/2025JD045745

Received 12 DEC 2025
Accepted 7 JUL 2026

Author Contributions:

Conceptualization: Fangmiao Xing
Data curation: Fangmiao Xing, Liang Ning, Fen Wu
Formal analysis: Liang Ning, Zhengyu Liu, Fen Wu, Lili Lei
Funding acquisition: Liang Ning, Jian Liu, Deliang Chen
Methodology: Fangmiao Xing, Liang Ning, Zhengyu Liu, Lili Lei, Yongjin Wang, Lingfeng Wan
Software: Lingfeng Wan
Supervision: Liang Ning, Jian Liu

Precipitation Reconstruction in the Asian Monsoon Region During the 4.2 ka Event With Paleoclimate Data Assimilation

Fangmiao Xing[1,2,3,4,5], Liang Ning[1,2,3,4,5], Zhengyu Liu[6], Jian Liu[1,2,3,4,5,7], Michael E. Mann[8], Fen Wu[1,2,3,4,5], Lili Lei[9,10], Yongjin Wang[1,2,3,4,5], Lingfeng Wan[11], Xin Jia[1,2,3,4,5], Hai Xu[12,13], Liangcheng Tan[14,15], Mi Yan[1,2,3,4,5], Weiyi Sun[1,2,3,4,5], Deliang Chen[16,17], Huayu Lu[18], Qin Wen[1,2,3,4,5], Kan Zhao[1,2,3,4,5], Kefan Chen[1,2,3,4,5], and Yanmin Qin[1,2,3,4,5]

[1]State Key Laboratory of Climate System Prediction and Risk Management, Nanjing, China, [2]Key Laboratory for Virtual Geographic Environment, Ministry of Education, Nanjing, China, [3]State Key Laboratory Cultivation Base of Geographical Environment Evolution and Regional Response of Jiangsu Province, Nanjing, China, [4]Jiangsu Center for Collaborative Innovation in Geographical Information Resource Development and Application, Nanjing, China, [5]School of Geography, Nanjing Normal University, Nanjing, China, [6]Department of Geography, The Ohio State University, Columbus, OH, USA, [7]Jiangsu Provincial Key Laboratory for Numerical Simulation of Large Scale Complex Systems, School of Mathematical Science, Nanjing Normal University, Nanjing, China, [8]Department of Earth and Environmental Science, Annenberg School for Communication, University of Pennsylvania, Philadelphia, PA, USA, [9]Key Laboratory of Mesoscale Severe Weather, Ministry of Education, and School of Atmospheric Sciences, Nanjing University, Nanjing, China, [10]Frontiers Science Center for Critical Earth Material Cycling, Nanjing University, Nanjing, China, [11]State Key Laboratory of Physical Oceanography, Ocean University of China, Qingdao, China, [12]Key Laboratory of Karst Georesources and Environment, Ministry of Education, College of Resources and Environmental Engineering, Guizhou University, Guiyang, China, [13]School of Earth System Science, Institute of Surface-Earth System Science, Tianjin University, Tianjin, China, [14]State Key Laboratory of Loess, Institute of Earth Environment, Chinese Academy of Sciences, Xi'an, China, [15]Institute of Global Environmental Change, Xi'an Jiaotong University, Xi'an, China, [16]Department of Earth System Sciences, Tsinghua University, Beijing, China, [17]Institute for Carbon Neutrality, Tsinghua University, Beijing, China, [18]School of Geography and Ocean Science, Nanjing University, Nanjing, China

Abstract For a long time, the 4.2 ka event was considered sufficiently significant to mark the onset of the Meghalayan Age, the latest stage of the Holocene. However, the spatial distribution and temporal evolutions of precipitation changes remain controversial in many regions, especially in monsoon Asia. In this study, combining the high-resolution speleothem calcite oxygen isotope ratio value ($\delta^{18}O_c$) records and the transient simulation of an isotope enabled earth system model, we reconstruct the spatiotemporal evolution of $\delta^{18}O_c$ and precipitation in the Asian monsoon region during the 4.2 ka event (4.3–3.9 ka BP) with 10-year temporal resolution and 2.5° × 1.9° spatial resolution, using an offline ensemble Kalman filter. Based on these reconstructed results, we analyze the characteristics of the 4.2 ka event over monsoon Asia from two aspects. On the centennial scale, the event shows a drought pattern in northern China and South Asia, and a wet pattern in southern China. On the multi-decadal scale, frequent wet-dry excursions occur in the region. Notably, both the centennial-scale changes and multi-decadal excursions largely fall within the range of Holocene natural variability. These results challenge the conventional view of the 4.2 ka event as a global megadrought and instead suggest that, even within monsoon Asia, it was expressed as a spatially heterogeneous hydroclimatic anomaly rather than a spatially uniform or exceptionally extreme event.

Plain Language Summary Researchers have long debated whether a significant global abrupt climate event occurred around 4,200 years ago. In the Asian monsoon region, in particular, the pattern of precipitation change remains uncertain. In this study, combining high-resolution paleoclimate proxy records and model simulations, we reconstruct precipitation changes in the Asian monsoon region over the last 11,000 years. With these results, we analyzed the hydroclimatic characteristics around 4,200 years ago over monsoon Asia from two aspects. On the centennial scale, drought spanned from northern China to South Asia, while southern China was wet. On a multidecadal scale, drought and flooding excursions frequently occur in the Asian monsoon region. Overall, these changes were spatially heterogeneous and generally remained within the range of natural Holocene variability, suggesting that the 4.2 ka event in monsoon Asia was not an exceptionally extreme or spatially uniform climate event.

Visualization: Fangmiao Xing
Writing – original draft: Fangmiao Xing, Liang Ning, Zhengyu Liu
Writing – review & editing: Fangmiao Xing, Liang Ning, Zhengyu Liu, Jian Liu, Michael E. Mann, Fen Wu, Lili Lei, Yongjin Wang, Lingfeng Wan, Xin Jia, Hai Xu, Liangcheng Tan, Mi Yan, Weiyi Sun, Deliang Chen, Huayu Lu, Qin Wen, Kan Zhao, Kefan Chen, Yanmin Qin

1. Introduction

Since the 4.2 ka event was identified and defined as a significant climatic abrupt event in the Holocene, numerous studies have sought to characterize its spatiotemporal patterns. By compiling global high-resolution proxy records, Weiss (2016) argued that the 4.2 ka event was a unique global-scale climate event manifested as a drought, second in magnitude only to the 8.2 ka event, but potentially twice as long in duration. Furthermore, since this time period coincides with significant transformation or collapse of several civilizations, such as the Akkadian Empire in Mesopotamia (Carolin et al., 2019; Weiss, 2016), Harappan Civilization in South Asia (Jahan & Quamar, 2024), and the Neolithic cultures in China (Chen et al., 2011; Gao et al., 2007; Jia et al., 2016, 2017, 2021; T. Wang et al., 2022; H. Zhang et al., 2021), it has continued to receive considerable attention.

However, over the past decade, more and more high-resolution proxy records have also provided an increasingly comprehensive description of the event, which has suggested a pattern contrary to the initially proposed "global megadrought" (James et al., 2025; McKay et al., 2024; Railsback et al., 2018; Renssen, 2022; Scroxton et al., 2023a, 2023b; Yang et al., 2021). Paleoclimatic proxies indicate a clear drought anomaly in mid-latitude regions of the Northern Hemisphere (Railsback et al., 2018; Renssen, 2022), but the broader spatial characteristic of the event remains uncertain. McKay et al. (2024) provided a particularly important benchmark for the present study by compiling 1,142 Holocene paleoclimate data sets and applying an objective framework to quantify the global significance of climate excursions. They found that, although some records show significant anomalies near 4.2 ka BP, these signals do not organize into large, coherent spatial regions, implying that the 4.2 ka interval is not remarkable at hemispheric to global scales in the context of Holocene variability. They also noted that previous characterizations of the event may have been influenced by confirmation bias and by inconsistent definitions of its timing and expression. James et al. (2025) employed three robust methods to investigate the expression of the 4.2 ka event, but all methods failed to detect spatially coherent variability consistent with a 4.2 ka event across Asia. Therefore, despite the growing number of high-resolution records, proxy evidence for the 4.2 ka event remains heterogeneous because different archives and indicators may record different aspects of hydroclimate, making it difficult to determine the sign, timing, and magnitude of precipitation or moisture changes at hemispheric and regional scales.

In the Asian monsoon region, the 4.2 ka climate event is more clearly reflected in proxy records, but its spatial characteristics remain debated. Across the East Asian monsoon region, it is still disputed whether the event followed a "northern dry/southern wet" pattern (Griffiths et al., 2020; Nan et al., 2025; Tan et al., 2018; H. Zhang et al., 2018) or showed a spatially consistent signal (McKay et al., 2024; Sun et al., 2019). Several proxy-based studies, particularly those using speleothem $\delta^{18}O_c$ records, proposed a centennial-scale "northern drought/southern flooding" pattern during the event (Griffiths et al., 2020; Nan et al., 2025; Tan et al., 2018; H. Zhang et al., 2018). In contrast, the compilation of proxy data by McKay et al. (2024) points to a more spatially heterogeneous hydroclimatic pattern in eastern China, with some records showing multi-decadal wet excursions.

Similar debates regarding the spatial and temporal characteristics of the 4.2 ka event also exist in the South Asian monsoon region. On the multidecadal-to-centennial scale, some proxy studies have characterized this interval as a prolonged drought lasting approximately two to three centuries (Berkelhammer et al., 2012; Dixit et al., 2014, 2018). This signal has often been hypothesized to reflect a weakening of the South Asian summer monsoon, although the climatic interpretation of speleothem $\delta^{18}O_c$ at suborbital timescales remains debated (J. Hu et al., 2019; Sinha et al., 2026). A high-resolution speleothem $\delta^{18}O_c$ record from Mawmluh Cave has been widely regarded as a key archive documenting this event (Berkelhammer et al., 2012). However, other high-resolution records suggest a more complex hydroclimatic structure (Kathayat et al., 2017, 2018; Scroxton et al., 2023b). For example, the Sahiya Cave record from northern India indicates an alternating sequence of cold/dry, warm/wet, and cold/dry conditions, rather than a single protracted drought (Kathayat et al., 2017). Together, these contrasting interpretations support the "Double Drying hypothesis", which challenges the view of a single continuous drought across the region during the 4.2 ka event.

While meta-analyses, such as that by McKay et al. (2024), have effectively compiled available proxy evidence to reveal the general modes of climate variability during the 4.2 ka event, significant uncertainties remain in the quantitative estimates of regional hydroclimate variables, such as precipitation. Furthermore, traditional methods of compiling and averaging proxy records often struggle to produce a continuous, dynamically consistent spatial evolution of an event with a fully quantified uncertainty framework. Climate models have thus far offered limited resolution to these debates because the mechanism of the 4.2 ka event remains unclear, and few simulation studies

Table 1
Information on the Speleothem Caves Used in This Study

No.	Abbreviation	Site name	Lat	Lon	Reference	Observation error variance (R)
1	ZZ	Zhenzhu	38.25	113.7	Li et al., 2020	0.092
2	LHN	Lianhua, shanxi	38.16667	113.7167	Dong et al. (2018)	0.249
3	BN	Baeg-nyong	37.27	128.58	Jo et al. (2017)	0.026
4	MG	Magou	34.3167	113.3833	Cai et al. (2021)	0.178
5	WY	Wuya	33.9167	105.4333	Tan et al. (2020)	0.093
6	DSY	Dongshiya	33.78333	111.5667	N. Zhang et al. (2018)	0.226
7	JX	Jiuxian	33.5667	109.1	Cai et al. (2010)	0.593
8	XL	Xianglong	33	106.33	Tan et al. (2018)	0.198
9	XN	Xiniu	31.679	110.42	J. Zhang et al. (2020)	0.141
10	SB	Sanbao	31.66667	110.4333	Dong et al. (2010)	0.063
11	HS	Heshang	30.45	110.4167	C. Hu et al. (2008)	0.140
12	LS	Luoshui	29.73	109.1167	Z. Wang et al., 2022b	0.074
13	SZ	Shizi	29.6822	106.2881	Yang et al. (2019)	0.123
14	LHS	Lianhua, hunan	29.48	109.5333	H. Zhang et al. (2013)	0.305
15	HF	Heifeng	29.0167	107.1792	Yang et al. (2019)	0.093
16	JF	Jinfo	29.0167	107.1792	Yang et al. (2019)	0.063
17	SN	Shennong	28.71	117.26	H. Zhang et al. (2021)	0.050
18	SG	Shigao	28.183	107.167	Jiang et al. (2012)	0.018
19	JL	Jiulong	27.8	113.9	H. Zhang et al. (2021)	0.077
20	DK	Dark	27.2	106.1667	Jiang et al., 2013	0.139
21	DG	Dongge	25.2833	108.0833	Y. Wang et al., 2005	0.029
22	Sahiya	Sahiya	30.6	77.8667	Kathayat et al. (2017)	0.053
23	Mawmluh	Mawmluh	25.2622	91.8817	Kathayat et al. (2018)	0.026
24	Qunf	Qunf	17.1667	54.3	Fleitmann et al. (2007)	0.073
25	Hoq	Hoq	12.5866	54.3543	Van Rampelbergh et al. (2013)	0.106

have successfully captured its characteristics (Ning et al., 2019; Yan & Liu, 2019). Here, we address this gap by applying paleoclimate data assimilation (PDA) to combine proxy records with an isotope-enabled climate simulation. Focusing on the Asian monsoon region, we reconstruct the spatial-temporal evolution of the 4.2 ka event by assimilating the speleothem $\delta^{18}O_c$ records across the Asian monsoon region with the simulation of the isotope-enabled Transient Climate of the Last 21,000 years (iTraCE) (He et al., 2021; Ning et al., 2025). This framework allows us to move beyond site-by-site proxy interpretation and to evaluate the magnitude, spatial coherence, and regional heterogeneity of hydroclimatic anomalies within a consistent reconstruction framework. We further analyze both the centennial-mean climate response and the occurrence of multi-decadal abrupt climate excursions during the 4.2 ka event.

2. Materials and Methods

2.1. Speleothem Oxygen Isotope Data

We used 25 speleothem oxygen isotope ($\delta^{18}O_c$) records from across the Asian monsoon region from the SISAL3.0 database (Speleothem Isotopes Synthesis and AnaLysis database version 3.0) (Kaushal et al., 2024). 21 records are located in Eastern Asia, and 4 in South Asia (Table 1 and Figure S1 in Supporting Information S1). According to McKay et al. (2024), the analysis of records with clear climate excursions showed that the median start and end times for the 4.2 ka event were 4.2 ka BP and 4.0 ka BP, respectively (McKay et al., 2024). To align with these median times and to accommodate typical dating errors in paleoclimate archives and our assimilated results, we define the 4.2 ka event period as spanning the interval from 4.3 ka BP to 3.9 ka BP.

Therefore, we screened the speleothem $\delta^{18}O_c$ records from the following aspects: (a) The speleothem $\delta^{18}O_c$ records should cover the 4.2 ka event (4.3–3.9 ka BP). (b) To reduce the error between speleothem $\delta^{18}O_c$ records in the same cave, only one speleothem $\delta^{18}O_c$ record with the highest temporal resolution and the longest coverage from each cave is used in the data assimilation. (c) The cave location must be within 0°N to 45°N and 40°E to 140°E. After the screening, 25 speleothem $\delta^{18}O_c$ records were assimilated. Then, to ensure a common chronology, the speleothem $\delta^{18}O_c$ records were resampled to a 10-year temporal resolution by averaging.

2.2. Independent Hydroclimate-Sensitive Records

Independent hydroclimate-sensitive records were compiled through meta-analysis (McKay et al., 2024), and we selected 24 records located in the Asian monsoon region. The archive types include terrestrial sediment, lake sediment, marine sediment, peat and speleothems. The climate signal of each record follows the interpretation described by the original authors and is classified into two types: drought and wetness. The detailed information for these records, including site metadata, reference, and climate interpretation, is provided in Table S2 in Supporting Information S1.

2.3. iTraCE Simulation

iTraCE Holocene (11–0 ka BP) simulation (Ning et al., 2025) is performed by the water isotope-enabled version of the Community Earth System Model version 1.3, which could capture the observed variations of water isotopes ($\delta^{18}O$ and δD) in the atmosphere, land, ocean, sea ice, and river runoff components (Brady et al., 2019; Stevenson et al., 2019). The atmosphere component is the Community Atmosphere Model 5.3 (Neale et al., 2010) and has a 2.5° longitude and 1.9° latitude spatial resolution with 30 hybrid vertical levels. The land component is the Community Land Model 4 (Oleson et al., 2010), with the same horizontal grid as the atmosphere and 10 vertical soil levels. The ocean component is the Parallel Ocean Program 2 (Smith et al., 2010), and the sea ice component is the Los Alamos Sea Ice Model 4 (Hunke, 2010) with nominal 1° displaced-pole grids and 60 vertical levels. The transient simulation we used is driven by all four external forcings, that is, ice-sheet and ocean bathymetry (Peltier et al., 2015), orbital parameters (Berger, 1978), greenhouse gas concentrations (Lüthi et al., 2008), and melting water flux, referred to as the baseline experiment (ICE + ORB + GHG + MWF). The iTraCE transient simulations enable a comprehensive model-data comparison study since the LGM (He et al., 2021; Ning et al., 2025; Seltzer et al., 2025). In our study, all variables from the iTraCE simulation used in this study have a temporal resolution of 10 years.

2.4. Paleoclimate Data Assimilation

The PDA method used in this study is the offline ensemble Kalman filter (EnKF) (Hakim et al., 2016), utilizing the Python package cfr (Zhu et al., 2024a, 2024b). The PDA method comprises four main components: proxy records, which provide indirect records of past climate variables; a prior state ensemble, which provides prior estimates of climate variables generated by model simulations; proxy system models (PSMs), which establish relationships between climate variables and proxy records; and the EnKF operator, which estimates climate variables through a weighted average of the model spatial fields and proxy information. The EnKF method solves the following equation to calculate an ensemble of climate states ($\boldsymbol{x}_a$) from prior states taken from a climate model ($\boldsymbol{x}_b$) and proxy records ($\boldsymbol{y}$):

$$\boldsymbol{x}_a = \boldsymbol{x}_b + \mathrm{K}(\boldsymbol{y} - \boldsymbol{y}_e) \tag{1}$$

$\boldsymbol{x}_b$ is an ensemble of climate states taken from model simulations by 100 ensemble members. Here, we randomly selected prior from the background period 11–0 ka BP.

$$y_e = \mathcal{H}(x_b) \tag{2}$$

A critical component of PDA is the mapping of prior climate state variables to the assimilated proxies. In this framework, $\boldsymbol{y}_e$ is a vector containing estimates of the proxies derived from the prior, and this is expressed mathematically by Equation 2. The operator $\mathcal{H}$ in Equation 2 (i.e., the forward model) ideally represents the complete set of processes associated with proxy values, that is, a comprehensive physically based PSM (Tardif et al., 2019). The development and use of PSMs have advanced rapidly, including the Proxy System Modeling tool (PRYSM, Dee et al., 2015) for water isotope measurements ($\delta^{18}O$, δD), the Measurement Error PSM (Fischer, 2024) successfully used on coral $\delta^{18}O$, and VS-Lite (Tolwinski-Ward et al., 2011) for tree-ring width. However, we did not incorporate any existing PSMs in the PDA framework for this study. Although some speleothem $\delta^{18}O_c$ PSMs are accessible, such as PRYSM (Dee et al., 2015), essential parameters such as the residence time and the Peclet number in PRYSM are not yet obtainable from the speleothem sites within our proxy records. For a direct comparison with the speleothem $\delta^{18}O_c$ records, here we transfer simulated precipitation $\delta^{18}O_p$ to speleothem $\delta^{18}O_c$ using a simplified forward transformation following He et al. (2021) (see detailed equations in Text S1 in Supporting Information S1).

$\boldsymbol{y}–\boldsymbol{y}_e$ is the innovation, which is the new information from the proxy records not already contained in the prior. This new information is weighted against the prior through the Kalman gain matrix:

$$K = BH^T\left[HBH^T + R\right]^{-1} \tag{3}$$

where B is the prior covariance matrix, R is the error covariance matrix for the proxy data, and H represents the linearized mapping from the prior climate state to proxy estimates. The observation error variance is defined as the variance of the anomaly subtracting the Holocene sub-orbital variation from the original time series. The Holocene sub-orbital variation is calculated as the cubic polynomial interpolation for each record. The observation error variance values for each proxy record are provided in Table 1. Before applying the data assimilation, following previous studies (Osman et al., 2021; Tierney et al., 2020), we performed a group of sensitivity experiments with different percentages of R (such as $R/2$, $R/5$, $R/10$, … in Table S1 in Supporting Information S1) used in the data assimilation, to select the most suitable uncertainty values. Based on the performances, $R/2$ is selected as the best estimation of the uncertainty and is then used in the following data assimilation.

Solutions for the ensemble mean $\overline{x_a}$, and perturbations x_a' for the single kth proxy y_k, are obtained from:

$$\bar{x}_a = \bar{x}_b + \frac{\mathfrak{w}_{\text{loc}} \diamond \text{cov}\left(x_b, \bar{y}_{e,k}\right)}{\text{var}\left(y_{e,k}\right) + R_k}\left(y_k - \bar{y}_{e,k}\right) \tag{4a}$$

$$x_a' = x_b' - \left[1 + \sqrt{\frac{R_k}{\text{var}\left(y_{e,k}\right) + R_k}}\right]^{-1} \frac{\mathfrak{w}_{\text{loc}} \diamond \text{cov}\left(x_b, \bar{y}_{e,k}\right)}{\text{var}\left(y_{e,k}\right) + R_k}\left(y_{e,k}'\right) \tag{4b}$$

where $y_{e,k}$ is the prior estimate of the proxy, R_k is the diagonal element of R corresponding to proxy y_k, and cov() and var() represent the covariance and variance functions, respectively. Here, the covariance terms capture only the linear statistical dependence within the ensemble. Thus, even if the underlying proxy-climate relationship is physically nonlinear, the EnKF update represents only its linear statistical component. Covariance localization, given by a Schur product denoted by $\circ$ in Equation 4b (i.e., element-wise multiplication), is a distance-weighted filter w_{loc} on the prior covariance matrix.

The ensemble of updated states is then recovered by combining the posterior ensemble mean and perturbations:

$$x_a = \bar{x}_a + x_a' \tag{5}$$

In this study, simulated $\delta^{18}O_c$ (transferred from $\delta^{18}O_p$) and precipitation are used as prior variables, and the posterior contains the same variables at the same 10-year temporal resolution consistent with speleothem $\delta^{18}O_c$ records. The posterior retains the same spatial resolution as the prior (2.5° in longitude and 1.9° in latitude). Covariance localization defines the farthest area where the proxy record can participate in assimilation. Here, it is set to 24,000 km, but the assimilated results are insensitive to this value, as shown in the sensitivity tests.

2.5. Validation With Speleothem $\delta^{18}O_c$

To assess the reliability of the assimilated results, we compared the reconstructed $\delta^{18}O_c$ to independent speleothem $\delta^{18}O_c$ records following Hakim et al. (2016). In this process, 75% of the records (18 records) are randomly sampled and used for assimilation, and the remaining 25% of the records (7 records) provide a source of independent verification. 71% of the variance in observed $\delta^{18}O_c$ changes between the early, middle and late

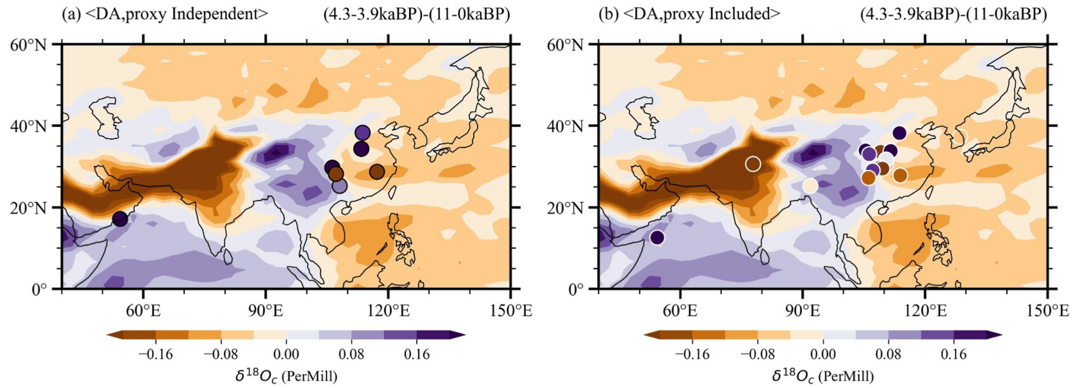

Figure 1. Validation of the DA reconstruction of $\delta^{18}O_c$ during the 4.2 ka event in the Asian Monsoon region. The figure indicates the mean values during 4.3–3.9 ka BP minus the mean during the background period (11–0 ka BP). The background shading in (a) and (b) shows the reconstructed $\delta^{18}O_c$ changes based on the paleoclimate data assimilation. Independent $\delta^{18}O_c$ records that were withheld from the DA are denoted by dotted symbols in (a), and $\delta^{18}O_c$ records used in DA are denoted in (b).

Holocene can be explained by the assimilated $\delta^{18}O_c$ results (Figure S2a in Supporting Information S1), compared with only 11% of the variance in observed $\delta^{18}O_c$ changes explained by the prior (Figure S2b in Supporting Information S1). The assimilated $\delta^{18}O_c$ changes share 3% of the variance with the simulated $\delta^{18}O_c$ changes (Figure S1c in Supporting Information S1). Overall, our reconstruction presents much better agreement with the speleothem $\delta^{18}O_c$ for the 4.2 ka event (Figure 1) than the iTraCE prior (Figure S3 in Supporting Information S1).

2.6. Anomaly Detection Methodology

To identify hydroclimatic anomalies associated with the 4.2 ka event, we employed a statistical framework adapted from McKay et al. (2024) and Morrill et al. (2013). We used the full Holocene (11–0 ka BP) as the background reference period because it provides a long-term context for evaluating hydroclimatic anomalies during the 4.2 ka interval. This provides a statistically robust baseline that captures the natural climate variability over the Holocene, after removing the orbital-scale trend.

First, each proxy record and data assimilation results were detrended over the full Holocene (11–0 ka BP) to remove orbital-scale variability and isolate multi-decadal to centennial signals. Second, the mean ($\bar{x}$) and standard deviation (σ) of the detrended Holocene series were calculated. Here, we applied two thresholds based on the detrended Holocene series: the $\pm 1\sigma$ range to identify enhanced anomalies from the Holocene background, and the $\pm 2\sigma$ range to identify extreme anomalies. Finally, we applied this framework to the 4.2 ka event interval (4.3–3.9 ka BP) at two temporal scales. For centennial-scale mean shifts, we compared the mean value of the 4.2 ka event interval to the Holocene mean and assessed whether the mean shift exceeded the $\pm 1\sigma$ or $\pm 2\sigma$ thresholds derived from the Holocene. For multi-decadal excursions, individual data points within the 4.2 ka interval were examined. Those falling outside the $\pm 1\sigma$ or $\pm 2\sigma$ bounds were considered anomalous. To avoid detecting spurious single-point spikes, a multi-decadal excursion was identified only if at least two adjacent anomalous values exhibited the same sign.

3. Results

3.1. Centennial Mean Shift in Speleothem $\delta^{18}O_c$ Records

The anomalous mean shifts of speleothem $\delta^{18}O_c$ in the Asian monsoon region are first calculated for the 4.2 ka event, with the Holocene period (11–0 ka BP) selected as the reference baseline (see details in Section 2.6). Among the 25 speleothem $\delta^{18}O_c$ records we selected, only 3 records (12% of the total) exhibit mean shifts during the 4.2 ka event exceeding of the $\pm 1\sigma$ range of baseline variability, with 2 showing depletion (negative) and 1 showing enrichment (positive) (Figure 2 and Figure S4 in Supporting Information S1). Of these, Dongshiya (DSY) cave shows a positive mean shift of 0.875‰, whereas Sanbao (SB) cave and Luoshui (LS) cave show negative mean shifts, with an average anomaly of −0.234‰. No record shows a mean shift exceeding $\pm 2\sigma$ range

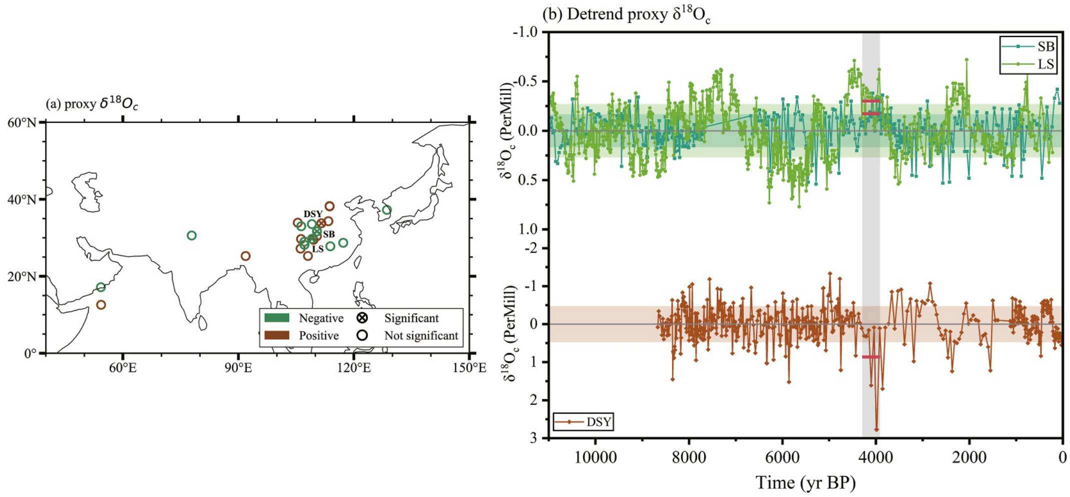

Figure 2. Mean shift of $\delta^{18}O_c$ in speleothem during the 4.2 ka event calculated from the detrended records as mean values during the 4.2 ka event (the gray shading, 4.3–3.9 ka BP) minus the mean of the Holocene background period (11–0 ka BP). (a) Spatial distributions of mean shifts in 25 speleothem $\delta^{18}O_c$ records. Green indicates depleting anomalies, brown indicates enriching anomalies, and the cross in the circle indicates that the anomaly exceeds one standard deviation of the detrended Holocene variability. (b) Detrended time series of the three speleothem $\delta^{18}O_c$ records whose mean shifts during the 4.2 ka event exceed $\pm 1\sigma$ range of the detrended Holocene variability. Green curves denote depleting anomalies, and brown curves denote enriching anomalies. For each record, the green and brown shading indicates $\pm 1\sigma$ ranges of its detrended Holocene background variability.

(Figure S4 in Supporting Information S1). Regionally, all records exceeding $\pm 1\sigma$ range are located in East Asia, while no speleothem record from South Asia exceeds this threshold.

In addition, the centennial scale anomalies in speleothem records are not spatially uniform even within East Asia, as both positive and negative mean shifts are identified. These results show that centennial-scale anomalies during the 4.2 ka event are detected only in a small subset of records, remain within the broader range of Holocene variability, and do not exhibit a coherent spatial pattern across the Asian monsoon region.

3.2. Centennial Anomaly of Reconstructed Precipitation

The mean shift of precipitation in the iTraCE simulation during the 4.2 ka event is not statistically significant across the Asian monsoon region based on the Student's *t*-test (Figure S5 in Supporting Information S1). However, because the relationship between $\delta^{18}O_c$ and the climate field in the model is constrained by physical equations, it can still be used to reconstruct precipitation using PDA. Compared with independent hydroclimate-sensitive records, including lake sediment and terrestrial sediment records (Table S2 in Supporting Information S1), we find that most records are consistent with the mean shift pattern of our reconstructed precipitation during the 4.2 ka event (Figure 3).

The assimilated precipitation results show that the 4.2 ka event is characterized by centennial scale drought in northern China and South Asia, and wetness in southeastern China and northwestern China, broadly consistent with the hydroclimate-sensitive records (Figure 3). The mean precipitation decrease in northern China is about −0.04 mm/day, corresponding to about −1.8% relative to the Holocene climatology, and that in South Asia is about −0.08 mm/day, corresponding to about −2.4%. Conversely, precipitation increased by an average of 0.06 mm/day in southeastern China, corresponding to about +1.2% (Figure 3 and Figure S7 in Supporting Information S1). However, although the assimilated precipitation anomalies during the 4.2 ka event are statistically significant (Figures S6 and S7 in Supporting Information S1), almost no region exceeds the $\pm 1\sigma$ range of the Holocene baseline variability (Figure 3). This suggests that the assimilated precipitation anomalies, while detectable in statistical terms, are generally modest relative to the magnitude of natural Holocene variability, and therefore do not indicate an exceptionally strong or spatially uniform precipitation anomaly across the Asian monsoon region.

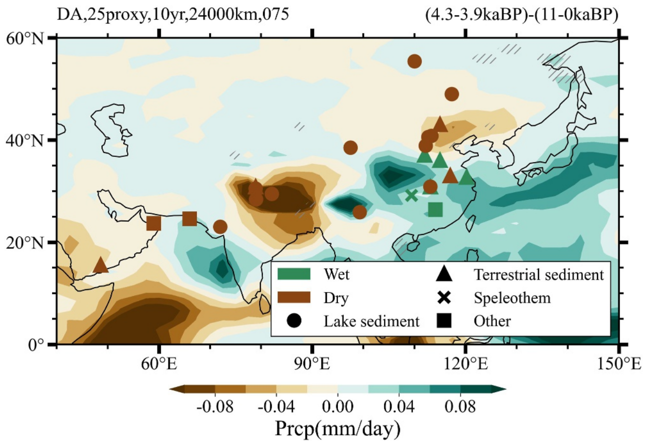

Figure 3. Mean shift of data assimilation precipitation during the 4.2 ka event in the Asian Monsoon region. The figure indicates the mean values during 4.3–3.9 ka BP minus the mean values during the background period (11–0 ka BP). The background shading shows the precipitation based on the paleoclimate data assimilation. The slash indicates that mean shifts during the 4.2 ka event exceed $\pm 1\sigma$ range of the detrended Holocene variability. Independent lake sediments, terrestrial sediments, speleothem records, and other records are shown as dots, triangles, crosses, and squares, respectively. Records indicating drier (wetter) conditions during the 4.2 ka event compared to the background period are colored brown (green).

3.3. Multi-Decadal Abrupt Climate Events During the 4.2 ka Event

In addition to the centennial-scale hydroclimatic shifts discussed above, the 4.2 ka interval was also characterized by pronounced variability at multi-decadal timescales, expressed as distinct positive and negative excursions in speleothem $\delta^{18}O_c$. To further assess the occurrence and significance of these short-term anomalies, we examined their expression during the 4.2 ka event (Figure 4).

More than 50% of the speleothem records we used exhibit multi-decadal excursions during the 4.2 ka event that exceed $\pm 1\sigma$ range of the Holocene baseline variability (Figure 4). However, only 6 out of 25 records exceed $\pm 2\sigma$ range. This indicates that multi-decadal excursions are relatively common during the 4.2 ka interval, but extreme events are restricted to a limited number of records. Regionally, positive excursions are mainly found in northern China, including Lianhua (LHN), Baegnyong (BN), Magou (MG), and Dongshiya (DSY) caves, whereas negative excursions are mainly recorded in central and southern China, including Jiuxian (JX), Sanbao (SB), Luoshui (LS), and Dongge (DG) caves. In South Asia, the records also display multi-decadal variability, but without a spatially consistent pattern. Overall, the multi-decadal signal is characterized by enrichment in northern China and depletion in central and southern China, although both positive and negative excursions may occur within individual records across the Asian monsoon region. Compared with the centennial-scale mean shifts, these results show that the 4.2 ka event is more clearly expressed at the multi-decadal scale, implying that short-lived anomalies may be muted in long-term averages. At the same time, the spatial heterogeneity of the excursions indicates that the event was not manifested as a uniform or synchronous hydroclimatic anomaly across the Asian monsoon region, while the small number of records exceeding $\pm 2\sigma$ range (Figure S8 in Supporting Information S1) suggests that most anomalies remained within or close to the range of natural Holocene variability.

For the assimilated results, we apply the same method to identify multi-decadal anomalies of the entire Asian monsoon region and its sub-regions. Based on regional averages, northern China, central China, and South Asia show precipitation decreases exceeding $\pm 1\sigma$ range of the Holocene background variability, whereas southern China shows increased precipitation, although the regional mean anomalies in all four regions remain within $\pm 2\sigma$ range (Figure 5b and Figure S9 in Supporting Information S1). While the regional averages highlight the broad contrasts in multi-decadal variability, they inevitably smooth over substantial spatial heterogeneity that exists within each subregion. A more detailed examination of the spatial patterns reveals the specific regional characteristics and timing of the multi-decadal excursions, for example, the different anomaly conditions between the east-west differences in South Asia, which are not evident from the regional averages alone (Figure 5a and Figure S10 in Supporting Information S1). In northern China, drought excursions occur during 4.2–4.1 ka BP and again during 4.0–3.9 ka BP. Central China experiences flooding excursions during 4.0–3.9 ka BP, particularly in the middle reach of the Yangtze River Basin. In southern China, drought and flooding excursions alternate through time, with wetter conditions dominating overall. In South Asia, the central and eastern parts are characterized by drought excursions during 4.2–4.0 ka BP, while the western parts show no clear excursions.

Taken together, the assimilated precipitation results indicate that the 4.2 ka event was characterized by regionally differentiated and temporally variable precipitation anomalies, rather than by a single spatially uniform monsoon response. Consistent with the speleothem $\delta^{18}O_c$ records, the assimilated precipitation fields show that the 4.2 ka event is more clearly expressed through multi-decadal excursions than through centennial-scale mean shifts, although the spatial pattern of these anomalies remains heterogeneous across the Asian monsoon region. These results suggest that the 4.2 ka event is better characterized as a series of sub-regional, multi-decadal excursions than by a coherent basin-wide anomaly persisting throughout the entire event interval.

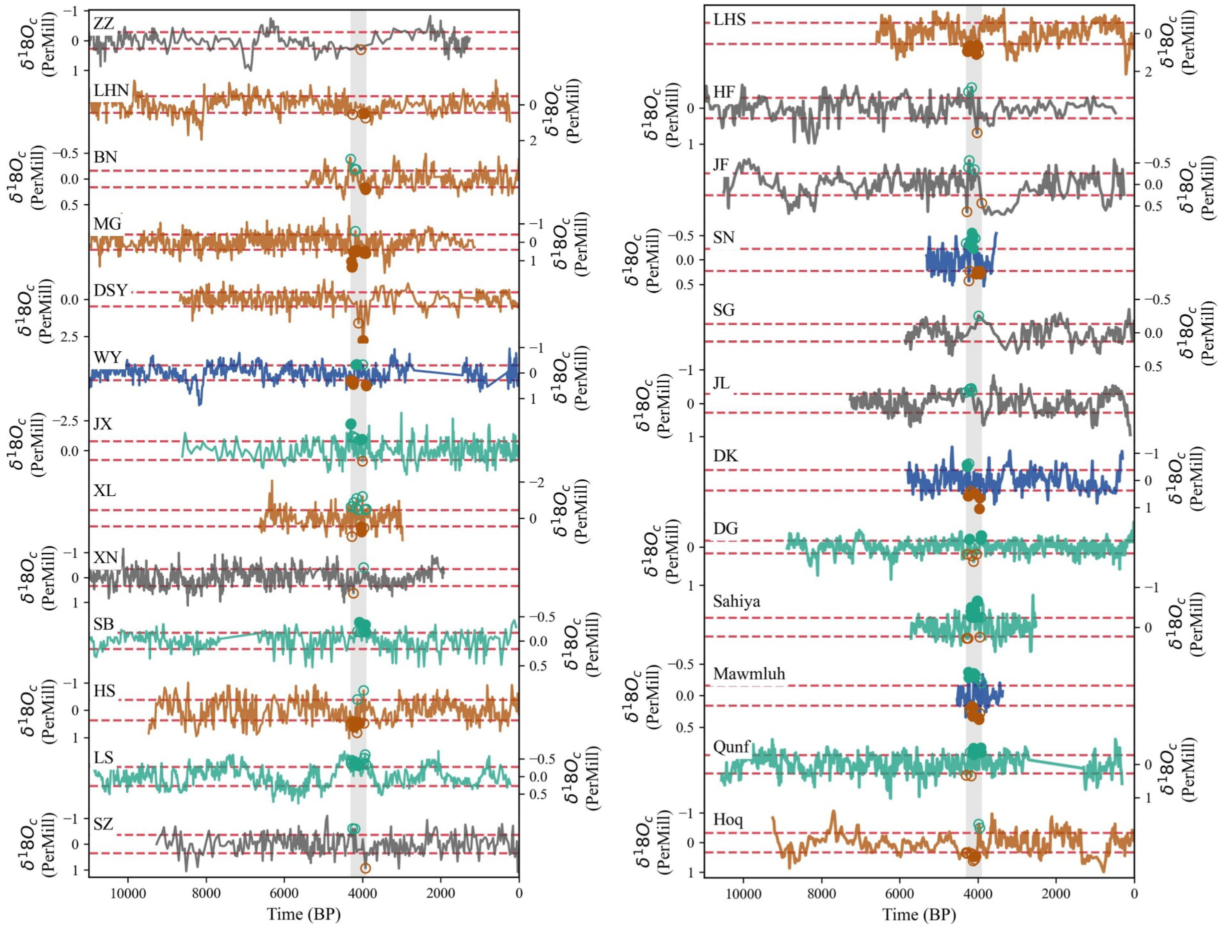

Figure 4. Multi-decadal excursions of speleothem $\delta^{18}O_c$ records in the Asian Monsoon region. The dashed red lines in each panel indicate the $\pm 1\sigma$ range of the detrended Holocene background variability (11–0 ka BP) used as the excursion detection criterion. Lines in green indicate that the $\delta^{18}O_c$ in speleothem has negative excursions, brown indicates that it has positive excursions, blue indicates the presence of both excursions, and black indicates no excursions. Solid dots indicate two consecutive points that exceed the value of the judgment criteria, that is, multi-decadal abrupt climate events, and hollow dots indicate only a single value that exceeds the threshold.

4. Discussion and Conclusion

In this study, our results indicate that hydroclimatic change during the 4.2 ka event in the Asian monsoon region is characterized by the co-existence of a weak centennial-scale mean-state shift and multi-decadal variability. At the centennial scale, precipitation mean shifts are statistically significant in some regions, but their magnitudes generally remain within 1σ of detrended Holocene background variability. This indicates that hydroclimatic change during the 4.2 ka interval involved a persistent directional shift, yet still largely remained within the range of detrended Holocene background variability. Circulation diagnostics support this interpretation. The anomalous 850-hPa and 200-hPa wind fields indicate a regional reorganization of the monsoon circulation background state during 4.3–3.9 ka BP (Figure S11 in Supporting Information S1). In eastern China, centennial-scale precipitation anomalies exhibit a south-wet/north-dry pattern, accompanied by an enhanced 200-hPa westerly jet, a weakened 850-hPa monsoon circulation, and contrasting vertical-motion anomalies, with negative 500-hPa omega over the south indicating enhanced ascent and positive omega over the north indicating enhanced subsidence (Figure S11 in Supporting Information S1). The vertically integrated moisture flux anomalies further show anomalous moisture convergence over southern China and moisture divergence over northern China, consistent with the south-wet/north-dry precipitation pattern. These results suggest that centennial-scale precipitation anomalies in eastern China were closely associated with the combined effects of anomalous vertical motion and regional moisture convergence/divergence under a reorganized circulation background state. In contrast, the drying over South Asia appears to be closely related to reduced moisture transport, together with anomalous moisture divergence over parts of the region (Figure S11c in Supporting Information S1). Taken together, these results

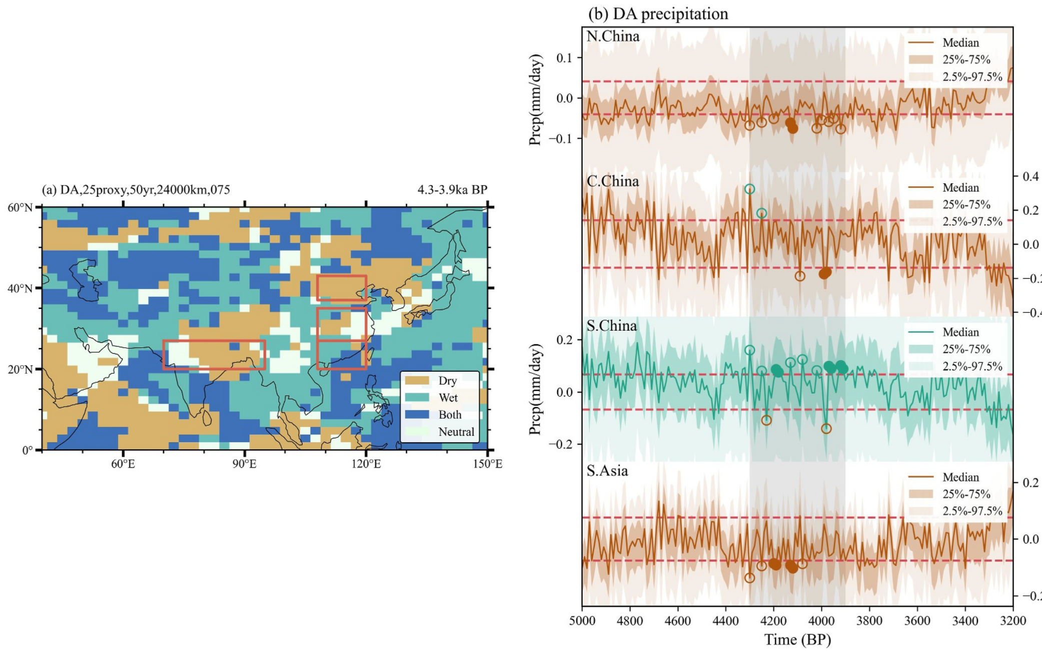

Figure 5. Spatiotemporal distribution of multi-decadal excursions of data assimilation precipitation. (a) Green indicates multi-decadal wet excursions exceeding $+1\sigma$ of the detrended Holocene background variability, brown indicates dry excursions exceeding -1σ, blue indicates the presence of both wet and dry excursions, and light mint green indicates no excursions exceeding $\pm1\sigma$. The red boxes mark the regions of northern China (N. China, 37–43°N, 108–120°E), Central China (C. China, 27–35°N, 108–120°E), southern China (S. China, 20–27°N, 108–120°E), and South Asia (S. Asia, 20–27°N, 70–95°E). (b) Area-averaged data assimilation precipitation over northern China, central China, southern China, and South Asia. The dark lines represent the medians, the darker shading indicates the inter-quartile range (25%–75% quantiles), and the lighter shading indicates the 95% interval (2.5%–97.5% quantiles). The dashed red lines in each panel indicate the $\pm1\sigma$ range of the detrended Holocene background variability (11–0 ka BP) used as the excursion detection criterion. Dots in (b) have the same meaning as Figure 4.

suggest that the centennial-scale mean shift of precipitation reflects regionally differentiated but generally moderate adjustments in moisture transport and mid-tropospheric vertical motion.

By contrast, at the multi-decadal scale, excursions exceeding 1σ occur across much of the Asian monsoon region, whereas excursions beyond 2σ are rare. This implies that the most prominent feature of the 4.2 ka event was not the frequent occurrence of widespread, persistent extremes, but rather the occurrence of short-term regional excursions within the range of Holocene variability. In this sense, the 4.2 ka event in the Asian monsoon region is better interpreted as multi-decadal regional excursions superimposed on a weak centennial-scale background shift, rather than as a spatially coherent and exceptionally intense hydroclimatic event.

This study has several limitations. First, speleothem $\delta^{18}O_c$ records are unevenly distributed across the Asian monsoon region, and proxy coverage remains sparse in some areas, which may weaken the constraints on reconstructed fields far from proxy sites. Second, the proxy records themselves contain uncertainties associated with chronology, non-climatic noise, and the climatic interpretation of speleothem $\delta^{18}O_c$. Third, although this study employed an offline PDA framework based on the EnKF, the reconstruction relies on linear covariance-based updates and may therefore not fully capture potentially nonlinear relationships between climate variables and speleothem $\delta^{18}O_c$. Future work could explore alternative DA approaches, such as machine learning and particle filters DA, which may better preserve such nonlinearities and could provide longer time series and higher resolution results. Future work integrating additional proxy types and reconstructing a wider range of climate variables may further improve both reconstruction skill and interpretation.

Conflict of Interest

The authors declare no conflicts of interest relevant to this study.

Availability Statement

All the assimilated proxies, code, and results are publicly available for downloading from Zenodo (Xing & Ning, 2026). All the speleothem $\delta^{18}O_c$ records were downloaded from the NOAA Paleoclimatology Data Archive (Kaushal et al., 2024). The iTraCE data were downloaded from the Climate Data Gateway at NCAR (Otto-Bliesner et al., 2024). The Python code used in this study is publicly available at Zenodo (Zhu et al., 2024a, 2024b).

Acknowledgments
This research was jointly supported by the National Key Research and Development Program of China (Grant 2023YFF0804704), the Science and Technology Innovation Project of Laoshan Laboratory (No. LSKJ202203300), and the National Natural Science Foundation of China (Grants 42130604, 42575050, 42475051, 42405056, and 42575051). DC was supported by Carbon Neutrality and Energy System Transformation (CNEST) Program and Tsinghua University (100008001).

References

Berger, A. (1978). Long-term variations of daily insolation and quaternary climatic changes. *Journal of the Atmospheric Sciences*, *35*(12), 2362–2367. https://doi.org/10.1175/1520-0469(1978)035<2362:ltvodi>2.0.co;2

Berkelhammer, M., Sinha, A., Stott, L., Cheng, H., Pausata, F. S. R., & Yoshimura, K. (2012). An abrupt shift in the Indian Monsoon 4000 years ago. *Climates, Landscapes, and Civilizations*, 75–88. https://doi.org/10.1029/2012GM001207

Brady, E., Stevenson, S., Bailey, D., Liu, Z., Noone, D., Nusbaumer, J., et al. (2019). The connected isotopic water cycle in the community Earth system model version 1. *Journal of Advances in Modeling Earth Systems*, *11*(8), 2547–2566. https://doi.org/10.1029/2019MS001663

Cai, Y., Cheng, X., Ma, L., Mao, R., Breitenbach, S. F. M., Zhang, H., et al. (2021). Holocene variability of East Asian summer monsoon as viewed from the speleothem δ18O records in central China. *Earth and Planetary Science Letters*, *558*, 116758. https://doi.org/10.1016/j.epsl.2021.116758

Cai, Y., Tan, L., Cheng, H., An, Z., Edwards, R. L., Kelly, M. J., et al. (2010). The variation of summer monsoon precipitation in central China since the last deglaciation. *Earth and Planetary Science Letters*, *291*(1), 21–31. https://doi.org/10.1016/j.epsl.2009.12.039

Carolin, S., Walker, R. T., Day, C., Ersek, V., Sloan, R. A., Dee, M., et al. (2019). Precise timing of abrupt increase in dust activity in the Middle East coincident with 4.2 ka social change. *Proceedings of the National Academy of Sciences*, *116*(1), 67–72. https://doi.org/10.1073/pnas.1808103115

Chen, D. D., Peng, S. Z., Zhang, W., Han, J. Q., & Ding, M. (2011). The response to Holocene climatic events of Shandong and their impacts on human activity. *Progress in Geography*, *30*, 846–852. (in Chinese).

Dee, S., Emile-Geay, J., Evans, M. N., Allam, A., Steig, E. J., & Thompson, D. M. (2015). Prysm: An open-source framework for PRoxY system modeling, with applications to oxygen-isotope systems. *Journal of Advances in Modeling Earth Systems*, *7*(3), 1220–1247. https://doi.org/10.1002/2015MS000447

Dixit, Y., Hodell, D. A., Giesche, A., Tandon, S. K., Gázquez, F., Saini, H. S., et al. (2018). Intensified summer monsoon and the urbanization of Indus Civilization in northwest India. *Scientific Reports*, *8*(1), 4225. https://doi.org/10.1038/s41598-018-22504-5

Dixit, Y., Hodell, D. A., & Petrie, C. A. (2014). Abrupt weakening of the summer monsoon in northwest India ∼4100 yr ago. *Geology*, *42*(4), 339–342. https://doi.org/10.1130/G35236.1

Dong, J., Shen, C.-C., Kong, X., Wu, C.-C., Hu, H.-M., Ren, H., & Wang, Y. (2018). Rapid retreat of the East Asian summer monsoon in the middle Holocene and a millennial weak monsoon interval at 9 ka in northern China. *Journal of Asian Earth Sciences*, *151*, 31–39. https://doi.org/10.1016/j.jseaes.2017.10.016

Dong, J., Wang, Y., Cheng, H., Hardt, B., Edwards, R. L., Kong, X., et al. (2010). A high-resolution stalagmite record of the Holocene East Asian monsoon from Mt Shennongjia, central China. *The Holocene*, *20*(2), 257–264. https://doi.org/10.1177/0959683609350393

Fischer, M. J. (2024). The Measurement Error Proxy System Model: MEPSM v0.2. *Geoscientific Model Development*, *17*(17), 6745–6760. https://doi.org/10.5194/gmd-17-6745-2024

Fleitmann, D., Burns, S. J., Mangini, A., Mudelsee, M., Kramers, J., Villa, I., et al. (2007). Holocene ITCZ and Indian monsoon dynamics recorded in stalagmites from Oman and Yemen (Socotra). *Quaternary Science Reviews*, *26*(1), 170–188. https://doi.org/10.1016/j.quascirev.2006.04.012

Gao, H., Zhu, C., & Xu, W. (2007). Environmental change and cultural response around 4200 cal. yr BP in the Yishu River Basin, Shandong. *Journal of Geographical Sciences*, *17*(3), 285–292. https://doi.org/10.1007/s11442-007-0285-5

Griffiths, M. L., Johnson, K. R., Pausata, F. S. R., White, J. C., Henderson, G. M., Wood, C. T., et al. (2020). End of Green Sahara amplified mid-to late Holocene megadroughts in mainland Southeast Asia. *Nature Communications*, *11*(1), 4204. https://doi.org/10.1038/s41467-020-17927-6

Hakim, G. J., Emile- Geay, J., Steig, E. J., Noone, D., Anderson, D. M., Tardif, R., et al. (2016). The last millennium climate reanalysis project: Framework and first results. *Journal of Geophysical Research: Atmospheres*, *121*(12), 6745–6764. https://doi.org/10.1002/2016jd024751

He, C., Liu, Z., Otto-Bliesner, B. L., Brady, E. C., Zhu, C., Tomas, R., et al. (2021). Hydroclimate footprint of Pan-Asian monsoon water isotope during the last deglaciation. *Science Advances*, *7*(4), eabe2611. https://doi.org/10.1126/sciadv.abe2611

Hu, C., Henderson, G. M., Huang, J., Xie, S., Sun, Y., & Johnson, K. R. (2008). Quantification of Holocene Asian monsoon rainfall from spatially separated cave records. *Earth and Planetary Science Letters*, *266*(3), 221–232. https://doi.org/10.1016/j.epsl.2007.10.015

Hu, J., Emile-Geay, J., Tabor, C., Nusbaumer, J., & Partin, J. (2019). Deciphering oxygen isotope records from Chinese speleothems with an isotope-enabled climate model. *Paleoceanography and Paleoclimatology*, *34*(12), 2098–2112. https://doi.org/10.1029/2019PA003741

Hunke, E. C. (2010). Thickness sensitivities in the CICE sea ice model. *Ocean Modelling*, *34*(3–4), 137–149. https://doi.org/10.1016/j.ocemod.2010.05.004

Jahan, T., & Quamar, M. F. (2024). The "4.2 ka drought event" and the fall of the Harappan Civilization: A critical review. *Review of Palaeobotany and Palynology*, *331*, 105187. https://doi.org/10.1016/j.revpalbo.2024.105187

James, A., Hu, J., Emile-Geay, J., Partin, J. W., Scroxton, N., Malik, N., & Gao, Y. (2025). Regime shifts in Holocene paleohydrology as recorded by Asian speleothems. *Paleoceanography and Paleoclimatology*, *40*(1), e2024PA004974. https://doi.org/10.1029/2024PA004974

Jia, X., Sun, Y., Wang, L., Sun, W., Zhao, Z., Lee, H. F., et al. (2016). The transition of human subsistence strategies in relation to climate change during the Bronze Age in the West Liao River Basin, Northeast China. *The Holocene*, *26*(5), 781–789. https://doi.org/10.1177/0959683615618262

Jia, X., Wang, S., Sun, Y., Li, Y., Jiao, Y., Zhao, Z., & Lee, H. F. (2021). Charcoal evidence for environmental change ca. 3.5 ka and its influence on ancient people in the West Liao River Basin of northeastern China. *Quaternary Research*, *102*, 142–152. https://doi.org/10.1017/qua.2020.120

Jia, X., Yi, S., Sun, Y., Wu, S., Lee, H. F., Wang, L., & Lu, H. (2017). Spatial and temporal variations in prehistoric human settlement and their influencing factors on the south bank of the Xar Moron River, Northeastern China. *Frontiers of Earth Science*, *11*(1), 137–147. https://doi.org/10.1007/s11707-016-0572-5

Jiang, X., He, Y., Shen, C., Kong, X., Li, Z., & Chang, Y. (2012). Stalagmite-inferred Holocene precipitation in northern Guizhou Province, China, and asynchronous termination of the Climatic Optimum in the Asian monsoon territory. *Chinese Science Bulletin*, *57*(7), 795–801. https://doi.org/10.1007/s11434-011-4848-6

Jiang, X., He, Y., Shen, C.-C., Li, Z., & Lin, K. (2013). Replicated stalagmite-inferred centennial-to decadal-scale monsoon precipitation variability in southwest China since the mid Holocene. *The Holocene*, *23*(6), 841–849. https://doi.org/10.1177/0959683612471986

Jo, K., Yi, S., Lee, J.-Y., Woo, K. S., Cheng, H., Edwards, L. R., & Kim, S.-T. (2017). 1000-Year quasi-periodicity of weak monsoon events in temperate Northeast Asia since the Mid-Holocene. *Scientific Reports*, *7*(1), 15196. https://doi.org/10.1038/s41598-017-15566-4

Kathayat, G., Cheng, H., Sinha, A., Berkelhammer, M., Zhang, H., Duan, P., et al. (2018). Evaluating the timing and structure of the 4.2 ka event in the Indian summer monsoon domain from an annually resolved speleothem record from Northeast India. *Climate of the Past*, *14*(12), 1869–1879. https://doi.org/10.5194/cp-14-1869-2018

Kathayat, G., Cheng, H., Sinha, A., Yi, L., Li, X., Zhang, H., et al. (2017). The Indian monsoon variability and civilization changes in the Indian subcontinent. *Science Advances*, *3*(12), e1701296. https://doi.org/10.1126/sciadv.1701296

Kaushal, N., Lechleitner, F. A., Wilhelm, M., Azennoud, K., Bühler, J. C., Braun, K., et al. (2024). SISALv3: A global speleothem stable isotope and trace element database. *Earth System Science Data*, *16*(4), 1933–1963. https://doi.org/10.5194/essd-16-1933-2024

Kaushal, N., Lechleitner, F. A., & Wilhelm, M., & SISAL working group members (n.d.). SISALv3: Speleothem Isotopes Synthesis and AnaLysis database version 3.0 [Dataset]. *NOAA Paleoclimatology Data Archive*. Retrieved from https://www.ncei.noaa.gov/pub/data/paleo/speleothem/SISAL-v3/

Li, Y., Rao, Z., Xu, Q., Zhang, S., Liu, X., Wang, Z., et al. (2020). Inter-relationship and environmental significance of stalagmite $\delta^{13}C$ and $\delta^{18}O$ records from Zhenzhu Cave, north China, over the last 130 ka. *Earth and Planetary Science Letters*, *536*, 116149. https://doi.org/10.1016/j.epsl.2020.116149

Lüthi, D., Le Floch, M., Bereiter, B., Blunier, T., Barnola, J.-M., Siegenthaler, U., et al. (2008). High-resolution carbon dioxide concentration record 650,000–800,000 years before present. *Nature*, *453*(7193), 379–382. https://doi.org/10.1038/nature06949

McKay, N. P., Kaufman, D. S., Arcusa, S. H., Kolus, H. R., Edge, D. C., Erb, M. P., et al. (2024). The 4.2 ka event is not remarkable in the context of Holocene climate variability. *Nature Communications*, *15*(1), 6555. https://doi.org/10.1038/s41467-024-50886-w

Morrill, C., Anderson, D. M., Bauer, B. A., Buckner, R., Gille, E. P., Gross, W. S., et al. (2013). Proxy benchmarks for intercomparison of 8.2 ka simulations. *Climate of the Past*, *9*(1), 423–432. https://doi.org/10.5194/cp-9-423-2013

Nan, Q., Chen, S., Liu, X., Ma, S., Sun, Y., Huang, L., et al. (2025). The 4.2 ka event in the Northern Hemisphere: Spatial heterogeneity and driving mechanisms of hydroclimatic change. *Earth-Science Reviews*, *265*, 105128. https://doi.org/10.1016/j.earscirev.2025.105128

Neale, R. B., Chen, C. C., Gettelman, A., Lauritzen, P. H., Park, S., Williamson, D. L., et al. (2010). Description of the NCAR Community Atmosphere Model (CAM5.0) (Tech. Rep. NCAR/TN-486+STR). *National Center for Atmospheric Research*

Ning, L., Liu, J., Bradley, R. S., & Yan, M. (2019). Comparing the spatial patterns of climate change in the 9th and 5th millennia BP from TRACE-21 model simulations. *Climate of the Past*, *15*(1), 41–52. https://doi.org/10.5194/cp-15-41-2019

Ning, L., Xing, F., Liu, Z., Liu, J., Mann, M. E., Wu, F., et al. (2025). Mega-Tripolar precipitation change accompanying water isotopes in Holocene Asian summer monsoon reanalysis. *Geophysical Research Letters*, *52*(17), e2025GL116451. https://doi.org/10.1029/2025GL116451

Oleson, K., Lawrence, D., Bonan, G., Flanner, M., Kluzek, E., Lawrence, P., et al. (2010). *Technical Description of version 4.0 of the Community Land Model (CLM)*. NSF National Center for Atmospheric Research. https://doi.org/10.5065/D6FB50WZ

Osman, M. B., Tierney, J. E., Zhu, J., Tardif, R., Hakim, G. J., King, J., & Poulsen, C. J. (2021). Globally resolved surface temperatures since the last Glacial Maximum. *Nature*, *599*(7884), 239–244. https://doi.org/10.1038/s41586-021-03984-4

Otto-Bliesner, B., Tomas, E. B. R., Liu, Z., & He, C. (2024). iTraCE [Dataset]. *Research Data Archive at the National Center for Atmospheric Research, Computational and Information Systems Laboratory*. https://doi.org/10.26024/b290-an76

Peltier, W. R., Argus, D. F., & Drummond, R. (2015). Space geodesy constrains ice age terminal deglaciation: The global ICE-6G_C (VM5a) model. *Journal of Geophysical Research: Solid Earth*, *120*(1), 450–487. https://doi.org/10.1002/2014JB011176

Railsback, L. B., Liang, F., Brook, G. A., Voarintsoa, N. R. G., Sletten, H. R., Marais, E., et al. (2018). The timing, two-pulsed nature, and variable climatic expression of the 4.2 ka event: A review and new high-resolution stalagmite data from Namibia. *Quaternary Science Reviews*, *186*, 78–90. https://doi.org/10.1016/j.quascirev.2018.02.015

Renssen, H. (2022). Climate model experiments on the 4.2 ka event: The impact of tropical sea-surface temperature anomalies and desertification. *The Holocene*, *32*(5), 378–389. https://doi.org/10.1177/09596836221074031

Scroxton, N., Burns, S. J., McGee, D., Godfrey, L. R., Ranivoharimanana, L., Faina, P., & Tiger, B. H. (2023a). Hydroclimate variability in the Madagascar and Southeast African summer monsoons at the Mid- to Late-Holocene transition. *Quaternary Science Reviews*, *300*, 107874. https://doi.org/10.1016/j.quascirev.2022.107874

Scroxton, N., Burns, S. J., McGee, D., Godfrey, L. R., Ranivoharimanana, L., Faina, P., & Tiger, B. H. (2023b). Tropical Indian Ocean basin hydroclimate at the Mid- to Late-Holocene transition and the double drying hypothesis. *Quaternary Science Reviews*, *300*, 107837. https://doi.org/10.1016/j.quascirev.2022.107837

Seltzer, A. M., Tyne, R. L., Musan, I., Langman, J. B., Amaya, D. J., Karnauskas, K. B., et al. (2025). Past aquifer responses to climate recorded by fossil groundwater. *Science Advances*, *11*(24), eadu7812. https://doi.org/10.1126/sciadv.adu7812

Sinha, A., Cheng, J., Li, H., Tanoue, M., Bong, H., Zhang, H., et al. (2026). ENSO modulated upstream convection as the primary control on interannual $\delta^{18}O$ variability in East Asia. *npj Climate and Atmospheric Science*, *9*(1), 64. https://doi.org/10.1038/s41612-026-01333-8

Smith, R., Jones, P., Briegleb, B. P., Bryan, F. O., Danabasoglu, G., Dennis, J. M., et al. (2010). The Parallel Ocean Program (POP) reference manual: Ocean component of the Community Climate System Model (CCSM). In *LAUR-01853* (Vol. 141, pp. 1–141). https://n2t.org/ark:/85065/d70g3j4h

Stevenson, S., Otto-Bliesner, B. L., Brady, E. C., Nusbaumer, J., Tabor, C., Tomas, R., et al. (2019). Volcanic eruption signatures in the isotope-enabled last millennium ensemble. *Paleoceanography and Paleoclimatology*, *34*(8), 1534–1552. https://doi.org/10.1029/2019PA003625

Sun, Q., Liu, Y., Wünnemann, B., Peng, Y., Jiang, X., Deng, L., et al. (2019). Climate as a factor for Neolithic cultural collapses approximately 4000 years BP in China. *Earth-Science Reviews*, *197*, 102915. https://doi.org/10.1016/j.earscirev.2019.102915

Tan, L., Cai, Y., Cheng, H., Edwards, L. R., Gao, Y., Xu, H., et al. (2018). Centennial- to decadal-scale monsoon precipitation variations in the upper Hanjiang River region, China over the past 6650 years. *Earth and Planetary Science Letters*, *482*, 580–590. https://doi.org/10.1016/j.epsl.2017.11.044

Tan, L., Li, Y., Wang, X., Cai, Y., Lin, F., Cheng, H., et al. (2020). Holocene monsoon change and abrupt events on the Western Chinese Loess Plateau as revealed by accurately dated stalagmites. *Geophysical Research Letters*, *47*(21), e2020GL090273. https://doi.org/10.1029/2020GL090273

Tardif, R., Hakim, G. J., Perkins, W. A., Horlick, K. A., Erb, M. P., Emile-Geay, J., et al. (2019). Last Millennium Reanalysis with an expanded proxy database and seasonal proxy modeling. *Climate of the Past*, *15*(4), 1251–1273. https://doi.org/10.5194/cp-15-1251-2019

Tierney, J. E., Zhu, J., King, J., Malevich, S. B., Hakim, G. J., & Poulsen, C. J. (2020). Glacial cooling and climate sensitivity revisited. *Nature*, *584*(7822), 569–573. https://doi.org/10.1038/s41586-020-2617-x

Tolwinski-Ward, S. E., Evans, M. N., Hughes, M. K., & Anchukaitis, K. J. (2011). An efficient forward model of the climate controls on interannual variation in tree-ring width. *Climate Dynamics*, *36*(11-12), 2419–2439. https://doi.org/10.1007/s00382-010-0945-5

Van Rampelbergh, M., Fleitmann, D., Verheyden, S., Cheng, H., Edwards, L., De Geest, P., et al. (2013). Mid- to late Holocene Indian Ocean Monsoon variability recorded in four speleothems from Socotra Island, Yemen. *Quaternary Science Reviews*, *65*, 129–142. https://doi.org/10.1016/j.quascirev.2013.01.016

Wang, T., Li, D., Cheng, X., Lan, J., Edwards, R. L., Cheng, H., et al. (2022a). Hydroclimatic changes in south-central China during the 4.2 ka event and their potential impacts on the development of Neolithic culture. *Quaternary Research*, *109*, 39–52. https://doi.org/10.1017/qua.2022.11

Wang, Y., Cheng, H., Edwards, R. L., He, Y., Kong, X., An, Z., et al. (2005). The Holocene Asian monsoon: Links to solar changes and north Atlantic climate. *Science*, *308*(5723), 854–857. https://doi.org/10.1126/science.1106296

Wang, Z., Chen, S., Wang, Y., Zhao, K., Liang, Y., Cheng, H., et al. (2022b). A high-resolution stalagmite record from Luoshui Cave, Central China over the past 23.5 kyr. *Quaternary Science Reviews*, *282*, 107443. https://doi.org/10.1016/j.quascirev.2022.107443

Weiss, H. (2016). Global megadrought, societal collapse and resilience at 4.2-3.9 ka BP across the Mediterranean and west Asia. *Past Global Change Magazine*, *24*(2), 62–63. https://doi.org/10.22498/pages.24.2.62

Xing, F., & Ning, L. (2026). Data for the paper: "Precipitation Reconstruction in the Asian Monsoon Region During the 4.2ka Event with Paleoclimate Data Assimilation" [Dataset]. *Zenodo*. https://doi.org/10.5281/zenodo.20729448

Yan, M., & Liu, J. (2019). Physical processes of cooling and mega-drought during the 4.2 ka BP event: Results from TraCE-21ka simulations. *Climate of the Past*, *15*(1), 265–277. https://doi.org/10.5194/cp-15-265-2019

Yang, B., Qin, C., Bräuning, A., Osborn, T. J., Trouet, V., Ljungqvist, F. C., et al. (2021). Long-term decrease in Asian monsoon rainfall and abrupt climate change events over the past 6,700 years. *Proceedings of the National Academy of Sciences*, *118*(30), e2102007118. https://doi.org/10.1073/pnas.2102007118

Yang, X., Yang, H., Wang, B., Huang, L.-J., Shen, C.-C., Edwards, R. L., & Cheng, H. (2019). Early-Holocene monsoon instability and climatic optimum recorded by Chinese stalagmites. *The Holocene*, *29*(6), 1059–1067. https://doi.org/10.1177/0959683619831433

Zhang, H., Cheng, H., Cai, Y., Spötl, C., Kathayat, G., Sinha, A., et al. (2018). Hydroclimatic variations in southeastern China during the 4.2 ka event reflected by stalagmite records. *Climate of the Past*, *14*(11), 1805–1817. https://doi.org/10.5194/cp-14-1805-2018

Zhang, H., Cheng, H., Sinha, A., Spötl, C., Cai, Y., Liu, B., et al. (2021). Collapse of the Liangzhu and other Neolithic cultures in the lower Yangtze region in response to climate change. *Science Advances*, *7*(48), eabi9275. https://doi.org/10.1126/sciadv.abi9275

Zhang, H., Yu, K., Zhao, J., Feng, Y., Lin, Y., Zhou, W., & Liu, G. (2013). East Asian Summer Monsoon variations in the past 12.5ka: High-resolution δ18O record from a precisely dated aragonite stalagmite in central China. *Journal of Asian Earth Sciences*, *73*, 162–175. https://doi.org/10.1016/j.jseaes.2013.04.015

Zhang, J., Kong, X., Zhao, K., Wang, Y., Liu, S., Wang, Z., et al. (2020). Centennial-scale climatic changes in Central China during the Holocene climatic optimum. *Palaeogeography, Palaeoclimatology, Palaeoecology*, *558*, 109950. https://doi.org/10.1016/j.palaeo.2020.109950

Zhang, N., Yang, Y., Cheng, H., Zhao, J., Yang, X., Liang, S., et al. (2018). Timing and duration of the East Asian summer monsoon maximum during the Holocene based on stalagmite data from North China. *The Holocene*, *28*(10), 1631–1641. https://doi.org/10.1177/0959683618782606

Zhu, F., Emile-Geay, J., Hakim, G. J., Guillot, D., Khider, D., Tardif, R., & Perkins, W. A. (2024a). cfr (v2024.1.26): A Python package for climate field reconstruction. *Geoscientific Model Development*, *17*(8), 3409–3431. https://doi.org/10.5194/gmd-17-3409-2024

Zhu, F., Emile-Geay, J., Hakim, G. J., Guillot, D., Khider, D., Tardif, R., & Perkins, W. A. (2024b). Cfr: A Python package for Climate Field Reconstruction (v2024.1.26) [Software]. *Zenodo*. https://doi.org/10.5281/zenodo.10575537

References From the Supporting Information

Berger, J.-F., Bravard, J.-P., Purdue, L., Benoist, A., Mouton, M., & Braemer, F. (2012). Rivers of the Hadramawt watershed (Yemen) during the Holocene: Clues of late functioning. *Quaternary International*, *266*, 142–161. https://doi.org/10.1016/j.quaint.2011.10.037

Cheng, Y., Shu, J., Hao, S., Gao, B., Li, X., Yuan, F., & Zou, X. (2023). Mid-to late Holocene vegetation response to relative sea-level fluctuations recorded by multi-proxy evidence in the Subei Plain, eastern China. *Palaeogeography, Palaeoclimatology, Palaeoecology*, *610*, 111327. https://doi.org/10.1016/j.palaeo.2022.111327

Coplen, T., Kendall, C., & Hopple, J. (1983). Comparison of stable isotope reference samples. *Nature*, *302*(5905), 236–238. https://doi.org/10.1038/302236a0

Cullen, H. M., de Menocal, P. B., Hemming, S., Hemming, G., Brown, F. H., Guilderson, T., & Sirocko, F. (2000). Climate change and the collapse of the Akkadian empire: Evidence from the deep sea. *Geology*, *28*(4), 379–382. https://doi.org/10.1130/0091-7613(2000)28<379:CCATCO>2.0.CO;2

Fairchild, I. J., & Baker, A. (2012). *Speleothem science: From process to past environments*. Wiley. Retrieved from https://searchworks.stanford.edu/view/965287

Fedotov, A., Vorobyeva, S., Vershinin, K., & Osipov, E. (2023). Climate changes in the south part of East Siberia for the last 5.5 ka inferred from multi-proxy sediment records of Lake Frolikha (Northern Baikal area, Russia). *Quaternary International*, *644–645*, 41–50. https://doi.org/10.1016/j.quaint.2021.11.021

Feng, M., Lü, T., Sun, J., & Cui, C. (2023). Optically stimulated luminescence dating and paleoclimatic implications of the Holocene dune sands in the Hunshandake Sandy Land, Northeast China. *Palaeogeography, Palaeoclimatology, Palaeoecology*, *615*, 111469. https://doi.org/10.1016/j.palaeo.2023.111469

Gao, W., Hu, H., Hou, W., Zhang, P., Gong, P., Jia, W., et al. (2022). The spatiotemporal patterns of human settlement during the longshan and erlitou periods in relation to extreme floods and subsistence strategy in the upper and middle Qin River reaches, central China. *Land*, *11*(7), 1088. https://doi.org/10.3390/land11071088

Hu, A., Meehl, G. A., Rosenbloom, N., Molina, M. J., & Strand, W. G. (2021). The influence of variability in meridional overturning on global Ocean circulation. *Journal of Climate*, *34*(18), 7697–7716. https://doi.org/10.1175/JCLI-D-21-0119.1

Jia, M., Li, C., Mao, X., Zhang, D., Wei, C., & Liu, H. (2021). Climate–human–environment interactions in the middle Yangtze Basin (central China) during the middle Holocene, based on pollen and geochemical records from the Sanfangwan Site. *Catena*, *204*, 105357. https://doi.org/10.1016/j.catena.2021.105357

Kotlia, B. S., & Joshi, L. M. (2013). Late Holocene climatic changes in Garhwal Himalaya. *Current Science*, *104*(7), 911–919. http://www.jstor.org/stable/24092104

Li, K., & Gao, W. (2021). Human settlement distribution patterns during the Longshan and Xinzhai-Erlitou periods and their hydrogeomorphic contexts in the Central Plains, China. *Catena*, *204*, 105433. https://doi.org/10.1016/j.catena.2021.105433

Lin, J., Jiang, W., Wang, L., Zhang, E., Tang, L., Yang, X., et al. (2022). Spatially diverse hydroclimatic response to the 4.2 ka event in the Asian monsoon region. *Quaternary Science Reviews*, *296*, 107809. https://doi.org/10.1016/j.quascirev.2022.107809

Moerman, J. W., Cobb, K. M., Partin, J. W., Meckler, A. N., Carolin, S. A., Adkins, J. F., et al. (2014). Transformation of ENSO-related rainwater to dripwater $\delta^{18}O$ variability by vadose water mixing. *Geophysical Research Letters*, *41*(22), 7907–7915. https://doi.org/10.1002/2014GL061696

Nakamura, A., Yokoyama, Y., Maemoku, H., Yagi, H., Okamura, M., Matsuoka, H., et al. (2016). Weak monsoon event at 4.2 ka recorded in sediment from Lake Rara, Himalayas. *Quaternary International*, *397*, 349–359. https://doi.org/10.1016/j.quaint.2015.05.053

O'Neil, J. R., Clayton, R. N., & Mayeda, T. K. (1969). Oxygen isotope fractionation in divalent metal carbonates. *The Journal of Chemical Physics*, *51*(12), 5547–5558. https://doi.org/10.1063/1.1671982

Pausata, F. S. R., Battisti, D. S., Nisancioglu, K. H., & Bitz, C. M. (2011). Chinese stalagmite $\delta^{18}O$ controlled by changes in the Indian monsoon during a simulated Heinrich event. *Nature Geoscience*, *4*(7), 474–480. https://doi.org/10.1038/ngeo1169

Prasad, S., & Enzel, Y. (2006). Holocene paleoclimates of India. *Holocene Climate and Cultural Evolution in Late Prehistoric-Early Historic West Asia*, *66*(3), 442–453. https://doi.org/10.1016/j.yqres.2006.05.008

Roy, I., Ranhotra, P. S., Tomar, N., Shekhar, M., Agrawal, S., Bhattacharyya, A., et al. (2022). Reconstruction of the late Holocene climate variability from the summer monsoon dominated Bhagirathi valley, western Himalaya. *Journal of Asian Earth Sciences*, *227*, 105080. https://doi.org/10.1016/j.jseaes.2022.105080

Shuchun, Y., Chunhai, L., Yangsheng, C., Yongfei, L., Lingyu, T., Ji, S., & Bin, X. (2022). Moisture conditions during the Younger Dryas and 4.2 ka event as revealed from a subalpine peat record in the Luoxiao Mountains, southern China. *Review of Palaeobotany and Palynology*, *305*, 104747. https://doi.org/10.1016/j.revpalbo.2022.104747

Singh, S., Gupta, A. K., Rawat, S., Bhaumik, A. K., Kumar, P., & Rai, S. K. (2022). Paleomonsoonal shifts during ~13700 to 3100 yr BP in the central Ganga Basin, India with a severe arid phase at ~4.2 ka. *Quaternary International*, *629*, 65–73. https://doi.org/10.1016/j.quaint.2021.01.015

Staubwasser, M., Sirocko, F., Grootes, P. M., & Segl, M. (2003). Climate change at the 4.2 ka BP termination of the Indus valley civilization and Holocene south Asian monsoon variability. *Geophysical Research Letters*, *30*(8). https://doi.org/10.1029/2002GL016822

Tian, F., Wang, Y., Zhao, Z., Li, Y., Dong, J., Liu, J., et al. (2020). Holocene vegetation and climate changes in the Huangqihai Lake Region, Inner Mongolia. *Acta Geologica Sinica. English Edition*, *94*(4), 1178–1186. https://doi.org/10.1111/1755-6724.14565

Wang, D., Li, M., Zhang, S., Xu, Q., & Wu, L. (2022c). Spatial and temporal characteristics of the precipitation response to the 4.2 ka event in the Asian summer monsoon region. *Global and Planetary Change*, *214*, 103854. https://doi.org/10.1016/j.gloplacha.2022.103854

Xiao, J., Zhang, S., Fan, J., Wen, R., Xu, Q., Inouchi, Y., & Nakamura, T. (2019). The 4.2 ka event and its resulting cultural interruption in the Daihai Lake basin at the East Asian summer monsoon margin. *Quaternary International*, *527*, 87–93. https://doi.org/10.1016/j.quaint.2018.06.025

Yan, D., & Wünnemann, B. (2014). Late Quaternary water depth changes in Hala Lake, northeastern Tibetan Plateau, derived from ostracod assemblages and sediment properties in multiple sediment records. *Quaternary Science Reviews*, *95*, 95–114. https://doi.org/10.1016/j.quascirev.2014.04.030

Zhang, G., Zhu, C., Wang, J., Zhu, G., Ma, C., Zheng, C., et al. (2010). Environmental archaeology on Longshan Culture (4500–4000 aBP) at Yuhuicun Site in Bengbu, Anhui Province. *Journal of Geographical Sciences*, *20*(3), 455–468. https://doi.org/10.1007/s11442-010-0455-8

Zhu, X. H., Li, B., Ma, C. M., Zhu, C., Wu, L., & Liu, H. (2017). Late Neolithic phytolith and charcoal records of human activities and vegetation change in Shijiahe culture, Tanjialing site, China. *PLoS One*, *12*(5), e0177287. https://doi.org/10.1371/journal.pone.0177287